# Resonance frequency of microbubbles: Effect of viscosity

Damir B. Khismatullin[a)]
*Department of Biomedical Engineering, Duke University, Durham, North Carolina 27708*

(Dated: April 19, 2004)

The transmitted frequency at which a gas bubble of millimeter or submillimeter size oscillates resonantly in a low-viscosity liquid is approximately equal to the undamped natural frequency (referred to as the Minnaert frequency if surface tension effects are disregarded). Based on a theoretical analysis of bubble oscillation, this paper shows that such an approximation cannot be validated for microbubbles used in contrast-enhanced ultrasound imaging. The contrast-agent microbubbles represent either encapsulated bubbles of size less than 10 $\mu$m or free (nonencapsulated) bubbles of submicron size. The resonance frequency of the microbubbles deviates significantly from the undamped natural frequency over the whole range of microbubble sizes due to the increased viscous damping coefficient. The difference between these two frequencies is shown to have a tremendous impact on the resonant backscatter by the microbubbles. In particular, the first and second harmonics of the backscattered signal from the microbubbles are characterized by their own resonance frequencies, equal to neither the microbubble resonance frequency nor the undamped natural frequency.

PACS numbers: 43.35.Ei, 43.80.Qf, 43.35.Bf

## I. INTRODUCTION

Due to its safety and low cost, ultrasound scanning, or echosonography, is actively used in obstetrics and gynecology. However it loses other imaging modalities in regard to the image quality. An excellent way to increase the quality of sonograms is the use of micron-size bubbles as ultrasound contrast agents,[1–3] i.e., as scatterers of ultrasound waves inside the human body. When injected into the bloodstream, the microbubbles, less than 10 $\mu$m in size, move with blood cells toward the measuring site. Once reached the blood vessel exposed to ultrasound, they break into oscillation and thus scatter the incoming ultrasound waves in all directions. Due to the large acoustic impedance difference at the interface between the gas and blood, scattering by microbubbles is of high intensity and results in a strong signal on the receiver, i.e., it enhances the echo from blood. Moreover, because microbubbles are nonlinear scatterers, the backscattered signal from them contains higher harmonics of the transmitted frequency. This has made possible the contrast harmonic imaging technique,[4,5] which, in the Doppler mode, can image blood flow in smallest blood capillaries, including myocardial perfusion.[3]

Although the overall effect of contrast agents on the backscattered signal can be easily detected, it is very difficult to measure oscillations of an individual microbubble in the population situated within the insonated blood vessel. The microbubble behavior can be recorded by optical imaging with a frame rate of several MHz. Such fast-speed imaging of contrast agent microbubbles has been reported by de Jong and co-workers.[6] This group of scientists measured the radius-time curves for microbubbles but did not relate these results to the contribution of each microbubble to the backscattered signal. In the absence of experimental data, we can only rely upon theory to realize how a given microbubble interacts with ultrasound. Particularly, a theoretical analysis of microbubble dynamics can be used (a) to evaluate the transmitted frequency at which scattering by a microbubble of a given size reaches the maximum and (b) to determine the intensity (scattering cross-section) and damping rate of the scattered wave produced by the microbubble. The acoustic response of the microbubble population located near the measuring site can be calculated from these functions of bubble size, if the size distribution of microbubbles in the population is known or has been measured.

All theoretical works concerning oscillations of ultrasound contrast agents are based on the Raleigh-Plesset equation.[7] A number of corrections to this model have been made, including the effects of the encapsulating shell,[8,9] blood compressibility[10] and viscoelasticity,[11] and interaction between microbubbles.[12] Hilgenfeldt *et al.*[13] analyzed theoretically the effects of nonlinearity and polychromaticity (pulsed driving) on the resonant backscatter by free microbubbles. Except for Refs. 11 and 13, these works analyze backscattering by contrast agents from the viewpoint of large bubbles. If a bubble is covered with a high-viscosity shell and its size is less than 10 $\mu$m, its resonance frequency differs significantly from its natural frequency due to the increased viscous damping coefficient.[11] For a free bubble, the shift in resonance frequency due to damping effects were discussed by Leighton[14] and Brennen.[15] As shown here, the difference between these two frequencies has a tremendous impact on backscattering by ultrasound contrast agents. For example, it is believed[1] that contrast-enhanced ultrasound provides images with the highest quality if it operates at the frequency at which the major part of microbubble population resonates. To put it differently, if the backscattered signal has a peak at the transmit-

a) Electronic address: damir@duke.edu

ted frequency or at multiple of this frequency, it comes from bubbles which resonate at this frequency. However, we will demonstrate that *the frequency at which the signal scattered by a microbubble has a resonance peak is not equal to the resonance frequency of the microbubble*.

The commercially available ultrasound contrast agents can be divided into two different types: (i) suspensions of encapsulated microbubbles and (ii) emulsions of liquid dodecafluoropentane (DDFP) and superheated drops. Encapsulated microbubbles are coated by a polymer,[1] protein,[1] or lipid layer[16] with the aim to increase stability of microbubbles in blood flow. The thickness and mechanical properties (viscosity and elasticity) of the layer differ for different contrast agents. An emulsion of liquid dodecafluoropentane[17] boils at 28° C, i.e., it becomes a suspension of free (non-encapsulated) microbubbles after intravenous injection. A superheated emulsion[18] also transforms itself into a suspension of free microbubbles but under the action of ultrasound. In this paper, the resonant properties of both free and encapsulated microbubbles are studied theoretically.

## II. ENCAPSULATED MICROBUBBLES

Free gas microbubbles dissolve away in blood very quickly. This is caused by the over-pressure in the gas inside the bubble compared to the pressure in blood due to surface tension at the gas-blood interface.[19] Encapsulation of the microbubble by a biocompatible surface-active layer lowers the over-pressure, and, as a result, makes the microbubble more stable against dissolution. The increased stability is the reason why the great bulk of available contrast agents represent encapsulated microbubbles. However, the encapsulating shell inevitably constrains the bubble oscillation due to the shell viscosity, which is much higher than the viscosity of blood plasma, and thus results in decreasing the amplitude of the backscattered signal. The shell-induced damping of the oscillation becomes more pronounced with increasing the shell thickness.[11]

The encapsulating shell shows viscoelastic properties. Elasticity of the shell material arises from changes in configurations of its macromolecules under flow.[20] The viscoelastic solid model of the shell, in the form of the Kelvin-Voigt constitutive equation, has been studied in Refs. 9 and 11. According to this model, the shell elasticity plays a positive role for scattering. An increase in the shell elasticity leads to increasing the magnitude of the resonance peaks in the scattering cross-section curves.[11] In this section, we analyze the effect of viscosity on the resonance frequency of and resonant backscatter from microbubbles encapsulated by a viscoelastic solid shell.

Let us consider a spherical gas bubble covered by a viscoelastic layer of finite thickness (Fig. 1). The bubble resides in an unbounded Newtonian liquid (blood plasma) and oscillates under the action of ultrasound. The radial oscillation of an encapsulated bubble is described by the equation[11]:

$$\rho_{s0}\left\{\left(1+\frac{\Delta_\rho a}{R}-\frac{F}{C_l}\frac{da}{dt}\right)a\frac{d^2a}{dt^2}+\left[\frac{3}{2}+\frac{\Delta_\rho a}{R}\left(2-\frac{a^3}{2R^3}\right)-\frac{1}{2C_l}\frac{d}{dt}(aF)\right]\left(\frac{da}{dt}\right)^2\right\}$$
$$=p_a-p_I+\frac{\rho_{l0}}{\rho_{s0}C_l}\frac{d}{dt}\left[\frac{a(p_a-p_I)}{1+\Delta_\rho a/R}\right], \tag{1a}$$

$$p_a=p_{g0}\left(\frac{a}{a_0}\right)^{-3\kappa}-2\left(\frac{\sigma_1}{a}+\frac{\sigma_2}{R}\right)+3\left[\int_a^R\frac{\tau_{rr}^{(s)}}{r}dr+\int_R^\infty\frac{\tau_{rr}^{(l)}}{r}dr\right]. \tag{1b}$$

Here $t$ is time, $a$ the inner radius of the bubble, $R$ the outer radius of the bubble ($d=R-a$ is the shell thickness), $\rho_{s0}$ the shell density, $\rho_{l0}$ the initial density of the liquid (blood plasma), $p_{g0}=p_0$ the initial gas pressure, $p_I$ the incident pressure in the liquid, and $C_l$ the speed of sound in the liquid. Surface tensions at the inner (gas-shell) and outer (shell-liquid) interfaces are denoted by $\sigma_1$ and $\sigma_2$. The parameters $\Delta_\rho$ and $F$ are defined as

$$\Delta_\rho=\frac{\rho_{l0}-\rho_{s0}}{\rho_{s0}},\quad F=\frac{\rho_{l0}}{\rho_{s0}}\frac{1+\Delta_\rho(a/R)^4}{1+\Delta_\rho a/R}. \tag{2}$$

A polytropic exponent $\kappa$ is different from $\gamma_g$ (ratio of constant-pressure to constant-volume specific heats for the gas) because of heat transfer through the bubble walls. It takes the value between 1 (isothermal behavior) and $\gamma_g$ (adiabatic behavior). However, we disregard the energy dissipation due to thermal effects because the thermal damping coefficient for an encapsulated microbubble is three orders of magnitude less than the viscous damping coefficient if the ultrasound scanner operates at frequencies $f=1$ - 10 MHz.[11] In the case of free microbubbles, thermal damping is two orders of magnitude less than viscous damping.[11]

The integrals in (1b) represent the contributions of the shell and liquid viscoelasticities to the bubble oscillation. The radial component of the shear stress tensor (radial stress) is denoted by $\tau_{rr}$. In the shell domain, $\tau_{rr}=\tau_{rr}^{(s)}$. In the liquid domain, $\tau_{rr}=\tau_{rr}^{(l)}$. The liquid elasticity weakly affects the bubble oscillation as compared to the shell elasticity.[11] Therefore, we assume that the liquid is Newtonian, i.e., $\tau_{rr}^{(l)}$ depends linearly on the radial component of the rate-of-strain tensor:

$$\tau_{rr}^{(l)}=2\mu_l\,\dot\gamma_{rr}=2\mu_l\frac{\partial v_r}{\partial r}. \tag{3}$$

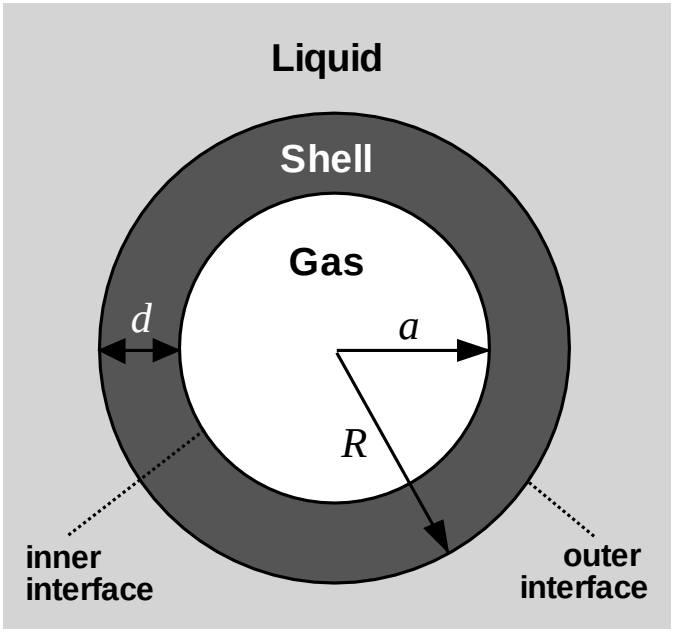


FIG. 1. Schematic sketch of an encapsulated microbubble of outer radius $R$. The microbubble resides in an unbounded Newtonian liquid. It is covered with a shell (viscoelastic layer of finite thickness $d$), i.e., it is characterized by two interfaces: inner (gas-shell) and outer (shell-liquid) interfaces.

($\mu_l$ is the liquid viscosity). Near the outer interface of the oscillating bubble, the radial velocity of the liquid is

$$v_r = \frac{a^2}{r^2}\frac{da}{dt} = \frac{R^2}{r^2}\frac{dR}{dt}. \tag{4}$$

Provided $\tau_{rr}^{(l)}\Big|_{r\to\infty} = 0$, substitution of Eqs. (3) and (4) into the second integral of Eq. (1b) gives

$$3\int_R^\infty \frac{\tau_{rr}^{(l)}}{r}dr = -\frac{4\mu_l a^2}{R^3}\frac{da}{dt} = -\frac{4\mu_l}{R}\frac{dR}{dt}. \tag{5}$$

We restrict our attention to the case of small-amplitude oscillation of the microbubble in the sinusoidal pressure field

$$p_I = p_0 - P_A\sin(\Omega t) = p_0 + \frac{P_A}{2}\left[i\exp(i\Omega t) + c.c.\right]. \tag{6}$$

Here $p_0$ is the undisturbed liquid pressure in the region far from the microbubble (blood pressure), $P_A$ the acoustic pressure amplitude, $\Omega$ the angular transmitted frequency [the transmitted frequency $f = \Omega/(2\pi)$]. The symbol $c.c.$ denotes complex conjugate. The acoustic pressure amplitude is far less than $p_0$, i.e., there exists a small parameter $\varepsilon_p$ such that $P_A = \varepsilon_p p_0 P$ and $P$ is a real number of the order of 1. Then, the solution to Eq. (1) is expanded in powers of $\varepsilon_p$ as[11]

$$a = a_0(1+x), \tag{7a}$$

$$R = R_0\left[1+\frac{a_0^3}{R_0^3}x + \frac{a_0^3}{R_0^3}\left(1-\frac{a_0^3}{R_0^3}\right)x^2 + O(x^3)\right], \tag{7b}$$

$$x = x(t;\varepsilon_p) = \varepsilon_p x_1(t) + \varepsilon_p^2 x_2(t) + O(\varepsilon_p^3) \tag{7c}$$

($a_0$ and $R_0$ are the equilibrium values of the inner and outer radii of the microbubble). The linear and second-order nonlinear acoustic responses of the microbubble (the first and second harmonics of microbubble oscillation) are specified by the functions $X_1(t) = \varepsilon_p a_0 x_1(t)$ and $X_2(t) = \varepsilon_p^2 a_0 x_2(t)$. They may be expressed as

$$X_1(t) = \frac{A_{1r}(\Omega)}{2}P_A\exp(i\Omega t), \tag{8a}$$

$$X_2(t) = A_{0r}(\Omega)P_A^2 + \frac{A_{2r}(\Omega)}{2}P_A^2\exp(2i\Omega t), \tag{8b}$$

where $A_{0r}(\Omega)$, $A_{1r}(\Omega)$, and $A_{2r}(\Omega)$ are the complex-valued functions of the transmitted frequency. The magnitudes of these functions represent the zeroth-, first-, and second-harmonic responses of the microbubble to the ultrasound field.

To calculate the contribution of the microbubble to the backscattered signal, the scattering cross-sections of the microbubble at the transmitted frequency and at twice the transmitted frequency are considered. The scattering cross-section at the transmitted frequency, or the first-harmonic scattering cross-section, is denoted by $\sigma_{s1}$. It is related to the ratio of the total acoustic power $W_1$ scattered by the microbubble at the first harmonic to the intensity $I_0$ of the incident acoustic field[9]:

$$\sigma_{s1} = \frac{W_1}{I_0}, \quad W_1 = \frac{4\pi r^2|P_{s1}|^2}{2\rho_l C_l}, \quad I_0 = \frac{P_A^2}{2\rho_l C_l}. \tag{9}$$

The symbol $\sigma_{s2}$ denotes the scattering cross-section at twice the transmitted frequency, or the second-harmonic scattering cross-section:

$$\sigma_{s2} = \frac{W_2}{I_0}, \qquad W_2 = \frac{4\pi r^2|P_{s2}|^2}{2\rho_l C_l}. \tag{10}$$

($W_2$ is the total acoustic power scattered by the microbubble at the second harmonic). Here $r$ is the radial coordinate, $P_{s1}$ and $P_{s2}$ are the first- and second-harmonic amplitudes of the pressure wave scattered by the microbubble. Based on the relationship between the scattered pressure field and the bubble radius[11,21–23]

$$p_s(t,r) = \frac{\rho_{l0}}{3r}\frac{d^2}{d\xi^2}a^3(\xi), \qquad \xi = t - r/C_l, \tag{11}$$

the expressions for $P_{s1}$ and $P_{s2}$ can be found [see Eqs. (86) and (87) in Ref. 11]. Then, the first- and second-harmonic scattering cross-sections depend on $A_{1r}(\Omega)$ and $A_{2r}(\Omega)$ as follows:

$$\sigma_{s1} = 4\pi\rho_{l0}^2 a_0^4\Omega^4|A_{1r}(\Omega)|^2, \tag{12a}$$

$$\sigma_{s2} = 64\pi\rho_{l0}^2 a_0^4 P_A^2\Omega^4\left|A_{2r}(\Omega) + \frac{A_{1r}^2(\Omega)}{2a_0}\right|^2. \tag{12b}$$

It is important to say that the expression for the second-harmonic scattering cross-section given by Church [Eq. (26b) in Ref. 9] is in error because it has been derived without considering (a) the nonlinear relationship between the scattered pressure field and bubble oscillation and (b) the dependence

of the scattered pressure on the second time derivative of the bubble radius. Due to the same reasons, it is also inappropriate to use the well-known formula for the scattered pressure[24]

$$p_s = i\Omega\rho_{l0}\left(a_0^2\frac{da}{dt}\right)\frac{\exp[-i(\Omega/C_l)r]}{r} \tag{13}$$

for evaluating nonlinear scattering by microbubbles.

If the shell behaves as a viscoelastic solid, its behavior can be described by the Kelvin-Voigt model. Because we ignore the shape deformation of the microbubble, this model is reduced to the following relation[11]:

$$\tau_{rr}^{(s)} = -\frac{4a^2}{r^3}\left[G_s(a-a_e)+\mu_s\frac{da}{dt}\right] \tag{14}$$

where $G_s$ and $\mu_s$ are the elasticity modulus and viscosity of the shell, $a_e$ is the unstrained inner radius of the bubble, which is different from the equilibrium radius $a_0$ due to radial pre-stress in the shell.[11] Under the assumption that the pre-stress is counterbalanced by the over-pressure, the unstrained radius depends on the shell elasticity and surface tensions[9]:

$$a_e = a_0(1+Z), \quad Z = \frac{1}{2G_s}\left(\frac{\sigma_1}{a_0}+\frac{\sigma_2}{R_0}\right)\frac{R_0^3}{R_0^3-a_0^3}. \tag{15}$$

In view of Eq. (15), substitution of Eq. (14) into the first integral of Eq. (1b) gives

$$\begin{aligned} 3\int_a^R \frac{\tau_{rr}^{(s)}}{r}dr &= -\frac{4(R_0^3-a_0^3)}{R^3}\left[G_s\left(1-\frac{a_0}{a}\right)+\frac{\mu_s}{a}\frac{da}{dt}\right] \\ &+ \frac{a_0R_0^3}{aR^3}\left(\frac{2\sigma_1}{a_0}+\frac{2\sigma_2}{R_0}\right), \end{aligned} \tag{16}$$

Because $R^3 = a^3 + R_0^3 - a_0^3$ due to the shell incompressibility, equations (1), (5) and (16) can be combined into a single ODE in the inner radius $a$ (or in the outer radius $R$). The resulting differential equation represents the mathematical model for radial oscillation of an encapsulated microbubble in a compressible Newtonian liquid provided the encapsulating shell behaves as a viscoelastic solid. By applying the perturbation technique [see Eqs (6)-(8)] to this model and using Eqs (12) , we obtain the following expressions for the first- and second-harmonic scattering cross-sections of the microbubble:

$$\sigma_{s1} = \frac{4\pi(1+\Delta_\rho a_0/R_0)^{-2}\rho_{l0}^2a_0^2\Omega^4}{\rho_{s0}^2\left\{\left[\Omega_0^2-\Omega^2+S_{ac}(\Omega)\right]^2+4\Omega^2\beta^2(\Omega)\right\}}, \tag{17a}$$

$$\sigma_{s2} = \frac{16\pi(1+\Delta_\rho a_0/R_0)^{-4}\rho_{l0}^2P_A^2\Omega^4\Gamma(\Omega)}{\rho_{s0}^4a_0^2\left\{\left[\Omega_0^2-\Omega^2+S_{ac}(\Omega)\right]^2+4\Omega^2\beta^2(\Omega)\right\}^2}. \tag{17b}$$

Here $\Omega_0 = 2\pi f_0$ and $f_0$ is the undamped natural frequency, i.e., the natural frequency of microbubble oscillation upon ignoring viscous damping and liquid compressibility:

$$\begin{aligned} f_0 &= \frac{1}{2\pi a_0\left[\rho_{s0}(1+\Delta_\rho a_0/R_0)\right]^{1/2}}\left\{3\kappa p_0-\frac{2\sigma_1}{a_0}-\frac{2\sigma_2a_0^3}{R_0^4}\right. \\ &\left.+4G_s\left(1-\frac{a_0^3}{R_0^3}\right)\left[1+\left(1+\frac{3a_0^3}{R_0^3}\right)Z\right]\right\}^{1/2}. \end{aligned} \tag{18}$$

The function $S_{ac}(\Omega)$ is the contribution of acoustic radiation to the bubble stiffness:

$$S_{ac}(\Omega) = \frac{T_{ac}^2\Omega^4}{1+T_{ac}^2\Omega^2}, \quad T_{ac} = \frac{\rho_{l0}a_0}{\rho_{s0}C_l}\left(1+\frac{\Delta_\rho a_0}{R_0}\right)^{-1}. \tag{19}$$

If thermal damping is ignored, the total linear damping coefficient $\beta(\Omega) = \beta_{vis} + \beta_{ac}(\Omega)$, where

$$\beta_{vis} = \frac{2}{\rho_{s0}a_0^2}\left(1+\frac{\Delta_\rho a_0}{R_0}\right)^{-1}\left[\mu_s\left(1-\frac{a_0^3}{R_0^3}\right)+\mu_l\frac{a_0^3}{R_0^3}\right], \tag{20}$$

$$\beta_{ac}(\Omega) = \frac{T_{ac}\Omega^2}{2(1+T_{ac}^2\Omega^2)} \tag{21}$$

are the viscous damping and acoustic radiation damping coefficients. The function $\Gamma(\Omega)$ can be written as

$$\Gamma(\Omega) = \frac{\left[\Omega_n^2-\alpha\Omega^2+S_n(\Omega)\right]^2+16\Omega^2\beta_n^2(\Omega)}{\left[\Omega_0^2-4\Omega^2+S_{ac}(2\Omega)\right]^2+16\Omega^2\beta^2(2\Omega)}. \tag{22}$$

Here

$$\alpha = \frac{3[1+\Delta_\rho(a_0/R_0)^4]}{2(1+\Delta_\rho a_0/R_0)}, \tag{23}$$

$$S_n(\Omega) = S_{ac}(2\Omega)-\frac{4\alpha}{3}\frac{T_{ac}^2\Omega^4(4+T_{ac}^2\Omega^2)}{(1+4T_{ac}^2\Omega^2)(1+T_{ac}^2\Omega^2)}, \tag{24}$$

$$\begin{aligned} \Omega_n &= \frac{1}{a_0\left[\rho_{s0}(1+\Delta_\rho a_0/R_0)\right]^{1/2}}\left\{\frac{9\kappa(\kappa+1)}{2}p_0\right. \\ &-\frac{4\sigma_1}{a_0}-\frac{4\sigma_2a_0^6}{R_0^7}+4G_s\left(1-\frac{a_0^3}{R_0^3}\right) \\ &\left.\times\left[2+\frac{3a_0^3}{R_0^3}+\left(2+\frac{3a_0^3}{R_0^3}+\frac{9a_0^6}{R_0^6}\right)Z\right]\right\}^{1/2}, \end{aligned} \tag{25}$$

$$\begin{aligned} \beta_n(\Omega) &= \frac{3}{\rho_{s0}a_0^2}\left(1+\frac{\Delta_\rho a_0}{R_0}\right)^{-1}\left[\mu_s\left(1-\frac{a_0^6}{R_0^6}\right)+\mu_l\frac{a_0^6}{R_0^6}\right] \\ &+\beta_{ac}(2\Omega)-\frac{\alpha}{2}\frac{T_{ac}\Omega^2(1-T_{ac}^2\Omega^2)}{(1+4T_{ac}^2\Omega^2)(1+T_{ac}^2\Omega^2)}, \end{aligned} \tag{26}$$

$F$ and $T_{ac}$ are given in Eqs (2) and (19), respectively.

By definition,[14] the linear resonance frequency of bubble oscillation $f_{res}$ is the frequency at which the bubble first-harmonic response (linear amplitude-frequency response) has a local maximum. If the bubble is covered with a shell, its first-harmonic response is of the form:

$$|A_{1r}(\Omega)| = \frac{\rho_{s0}^{-1}a_0^{-1}(1+\Delta_\rho a_0/R_0)^{-1}}{\left\{\left[\Omega_0^2-\Omega^2+S_{ac}(\Omega)\right]^2+4\Omega^2\beta^2(\Omega)\right\}^{1/2}}, \tag{27}$$

Even if the surrounding liquid is assumed to be incompressible, the total damping coefficient is sufficient large to influence the resonance frequency of microbubbles encapsulated by the high-viscosity shell. Damping has a negligible effect on $f_{res}$ if

$$\beta(\Omega) \ll \Omega_0/2 \tag{28}$$

This condition is satisfied if the Reynolds numbers for the shell $\mathrm{Re}_s = a_0\rho_{s0}U/\mu_s$ and for the liquid $\mathrm{Re}_l = a_0\rho_{l0}U/\mu_l$ are much more than unity ($U = \sqrt{p_0/\rho_{l0}}$ is the characteristic velocity). It is clear that the difference between the resonance and undamped natural frequencies increases with decreasing the bubble size and increasing viscosity. For microbubbles of radius 1 $\mu$m suspended in water and encapsulated by the shell, which density is equal to the water density, $Re_s < 1$ if $\mu_s > 0.01$ Pa·s $= 10$ cP. Meanwhile, the shell viscosity of contrast microbubbles is much higher than 10 cP.[8,25] Therefore, using the term "resonance frequency" as a synonym of "natural frequency" is validated only for large bubbles.

Upon neglecting the liquid compressibility, the simple expression for the resonance frequency is obtained from the maximization of $|A_{1r}(\Omega)|$:

$$f_{res} = f_{res0} = \sqrt{f_0^2 - \frac{\beta_{vis}^2}{2\pi^2}}\,. \tag{29}$$

As follows from Eq. (27), microbubbles resonate in a compressible viscous liquid at the frequency

$$f_{res} = \frac{1}{2\pi T_{ac}}\left\{-1 + \left[1 + \frac{4T_{ac}^2(2\pi^2 f_0^2 - \beta_{vis}^2)}{1 + 4T_{ac}\beta_{vis}(1+T_{ac}\beta_{vis})}\right]^{1/2}\right\}^{1/2}. \tag{30}$$

Note that the acoustic contribution to the resonance frequency of free bubbles was discussed by Prosperetti.[26]

Figure 2 compares the resonance frequency with the undamped natural frequency for air microbubbles encapsulated by the shell of viscosity $\mu_s = 0.45$ Pa·s and elasticity $G_s = 12$ MPa. The shell thickness $d$ is 5% of the initial outer radius $R_0$. As estimated by Hoff *et al.*,[25] these values of parameters are typical of "polymeric microbubbles" prepared by Nycomed.[27] We assume that the microbubbles reside in blood plasma (viscosity $\mu_l = 0.0012$ Pa·s, density $\rho_{l0} = 1027$ kg·m$^{-3}$, and speed of sound $C_l = 1543$ m·s$^{-1}$).[28] The shell density is supposed to be slightly higher than the plasma density: $\rho_{s0} = 1100$ kg·m$^{-3}$. The initial pressure in the liquid $p_0 = 0.1$ MPa. The surface tensions $\sigma_1 = 0.04$ N·m$^{-1}$ and $\sigma_2 = 0.005$ N·m$^{-1}$ (see Ref. 9). In the case of encapsulated microbubbles, the best matching between the numerical solution, which accounts for heat conduction through the bubble wall, and the analytical formula is observed at $\kappa = 1.1$.[11] This value of the polytropic exponent is used in all calculations here.

As illustrated in Fig. 2, there is a notable difference between the resonance and undamped natural frequencies over the whole range of microbubble sizes. In the case of Nycomed suspension, this difference varies from -0.39 MHz (15.9%) at $R_0 = 5$ $\mu$m to -3.30 MHz (141.8%) at $R_0 = 2.5$ $\mu$m. In addition, encapsulated microbubbles are characterized by a critical size below which they never resonate. The critical size is in the size range of contrast agents. The critical radius of Nycomed microbubbles is 2.24 $\mu$m. From both Eqs. (29) and (30) it follows that microbubbles cease to resonate if

$$\beta_{vis} \geq \pi\sqrt{2} f_0. \tag{31}$$

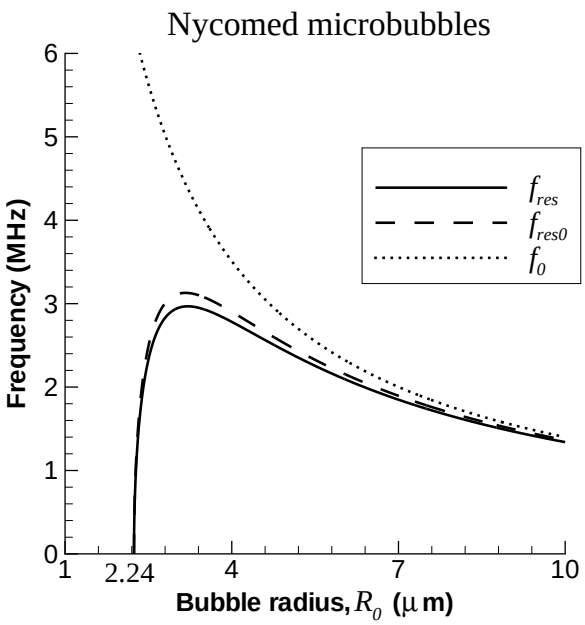


FIG. 2. Resonance frequency (solid) of an air microbubble encapsulated by a polymeric shell[25,27] as a function of the outer radius of the microbubble, compared with the undamped natural frequency (dotted). The microbubble resides in human blood plasma. The dashed line is the resonance frequency under the assumption that blood plasma is incompressible [Eq. (29)]. The solid and dotted lines are calculated from Eqs. (30) and (18), respectively. The encapsulating shell is characterized by viscosity of 0.45 Pa·s and elasticity of 12 MPa. Its thickness is 5% of the bubble outer radius. Other parameters: $\mu_l = 0.0012$ Pa·s, $C_l = 1543$ m·s$^{-1}$, $\rho_{l0} = 1027$ kg·m$^{-3}$, $\rho_{s0} = 1100$ kg·m$^{-3}$, $p_0 = 0.1$ MPa, $\sigma_1 = 0.04$ N·m$^{-1}$, $\sigma_2 = 0.005$ N·m$^{-1}$, and $\kappa = 1.1$.

The more the shell and liquid viscosities, the more the critical radius (and hence the difference between the resonance and undamped natural frequencies). Although the critical radius decreases with increasing the shell elasticity, the shell viscosity is a more important parameter: a ten-fold decrease in shell viscosity has approximately the same effect on the critical radius of Nycomed microbubbles as a 100-fold increase in shell elasticity.

Figure 2 also shows that ignoring the liquid compressibility leads to overestimation of the resonance frequency: the microbubble situated in a less compressible liquid resonates at a higher frequency. This happens due to acoustic radiation damping. The difference between $f_{res0}$ and $f_{res}$ reaches 0.165 MHz ($\approx 5.6\%$) for Nycomed bubbles of radius 3.1 $\mu$m. Another result of Fig. 2 is that there exists an upper limit to the resonance frequency of microbubbles: the Nycomed suspension does not resonate if the transmitted frequency exceeds 3 MHz. This result is, however, not applicable to the backscattered signal produced by the suspension, as shown later.

Even in the case of Albunex®, which is a suspension of protein-encapsulated microbubbles, there is a significant deviation of the resonance frequency from the undamped natural frequency for all possible sizes of microbubbles.[11] As es-

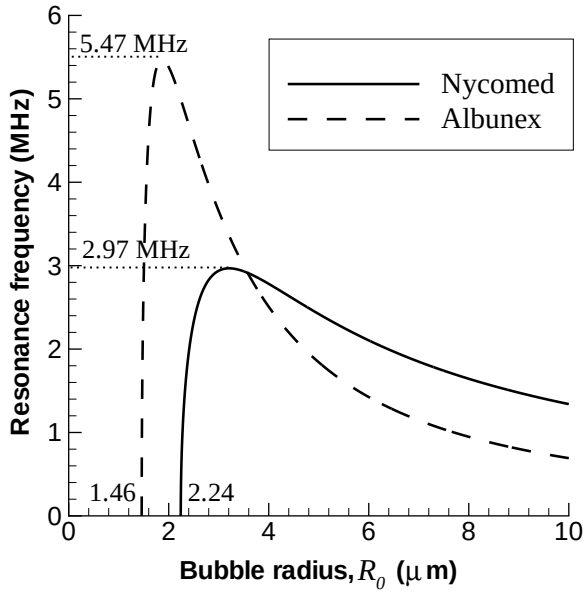


FIG. 3. Resonance frequencies of Nycomed and Albunex® microbubbles (solid and dashed) as functions of the outer radius [based on Eq. (30)]. The Albunex® microbubble is encapsulated by a protein shell of viscosity $\mu_s = 1.77$ Pa·s, elasticity $G_s = 88.8$ MPa, and constant thickness $d = 15$ nm (see Ref.9). Both microbubbles reside in human blood plasma. The parameters of the Nycomed microbubble and blood plasma are as in Fig. 2.

timated by Church,[9] the protein (albumin) shell of these microbubbles is thin ($d = 15$ nm), very viscous ($\mu_s = 1.77$ Pa·s) and elastic ($G_s = 88.8$ MPa). Figure 3 shows that the critical radius of Albunex® bubbles $R_c = 1.46$ $\mu$m. This value is less than the critical radius of Nycomed bubbles mainly due to a difference in shell thickness between these two contrast agents. The upper limit to the resonance frequency is higher for Albunex® ($f_{res}^{max} = 5.47$ MHz) than for Nycomed ($f_{res}^{max} = 2.97$ MHz). This can be explained only by a higher elasticity of the albumin shell. (A decrease in shell thickness leads to a decrease in the critical radius but has no effect on the upper limit to the resonance frequency.)[11]

The widely used assumption that the resonances of the backscattered signal (resonance peaks in the output-level versus frequency curve) are produced by microbubbles resonating at the transmitted frequency may lead to misinterpretation of experimental data. The first-harmonic resonance of the signal scattered by an encapsulated microbubble occurs at the frequency $f_1$, which is different from the resonance frequency of the microbubble $f_{res}$. If the surrounding liquid is considered to be incompressible, the maximization of the first-harmonic scattering cross-section $\sigma_{s1}$ [see Eq. (17a)] gives the following formula for $f_1$:

$$f_1 = \frac{f_0^2}{f_{res0}} = \frac{f_0^2}{\sqrt{f_0^2 - \beta_{vis}^2/(2\pi^2)}}. \tag{32}$$

In the case of large bubbles, i.e., when the difference between the resonance and undamped natural frequencies of bubble oscillation is negligible small, it is correctly reasoned that $f_1 = f_{res} = f_0$. In such a situation, resonating bubbles are responsible for the resonance peaks in the output-level versus frequency curve. In the case of small bubbles, the viscous damping coefficient is large and, therefore, nonresonating bubbles make the major contribution to the resonant backscatter.

Considering the liquid compressibility, the first-harmonic resonance frequency of the backscattered signal $f_1 = \sqrt{X}$. The quantity $X$, as is evident from the maximization of $\sigma_{s1}$, is one of the positive real roots of the cubic equation

$$X^3 + c_2 X^2 + c_1 X + c_0 = 0 \tag{33}$$

with

$$c_0 = \frac{f_0^4}{2\pi^2 T_{ac}^2 (1 + 2T_{ac}\beta_{vis})^2}, \tag{34a}$$

$$c_1 = \frac{8\pi^2 T_{ac}^2 f_0^4 + \beta_{vis}^2/(2\pi^2) - f_0^2}{2\pi^2 T_{ac}^2 (1 + 2T_{ac}\beta_{vis})^2}, \tag{34b}$$

$$c_2 = \frac{2(4\pi^2 T_{ac}^2 f_0^4 + \beta_{vis}^2/\pi^2 - 2f_0^2)}{(1 + 2T_{ac}\beta_{vis})^2}. \tag{34c}$$

Figure 4(a) plots the resonance and undamped natural frequencies of the Nycomed microbubble (dash-dot and dashed lines) situated in blood plasma as well as the first-harmonic resonance frequency of the signal scattered by the microbubble (solid line) as functions of the outer radius $R_0$. The first-harmonic resonance frequency is calculated from the solution of Eq. (33) (see p. 17 in Ref. 29). Like the undamped natural frequency $f_0$, the first-harmonic resonance frequency of the backscattered signal $f_1$ decreases monotonically with increasing the bubble radius. However, $f_0$ tends to infinity when the inner radius $a_0$ approaches zero, while $f_1$ reaches the highest value (several tens of MHz) at $a_0 > 0$. If we continue to use the assumption $f_1 = f_{res} = f_0$ for bubbles of arbitrary small size, we will be led to the conclusion that the bubble resonance and the resonance peak in the first-harmonic scattering cross-section always exist, no matter how bubbles are small. We will, then, argue that very small bubbles resonate at very high frequencies. Figure 4 demonstrates that this conclusion is wrong. Bubbles are characterized by the critical radius. Not only bubbles of subcritical size cease to resonate, but they also never produce the resonant backscatter at the transmitted frequency. (As will be shown later, bubbles of subcritical size can produce the resonant backscatter at twice the transmitted frequency.) The difference between the first-harmonic resonance frequency of the backscattered signal and the microbubble resonance frequency always exceeds the difference between the undamped natural and resonance frequencies of the microbubble. For Nycomed bubbles of outer radius $R_0 = 5$ $\mu$m, $f_1 - f_{res} \approx 0.73$ MHz (30.0%), while $f_0 - f_{res} \approx 0.38$ MHz (15.9%). If $R_0 = 2.54$ $\mu$m, $f_1 - f_{res} \approx 11.89$ MHz (487.2%) and $f_0 - f_{res} \approx 3.09$ MHz (126.8%).

As indicated in Fig. 4(b), a restriction on the first-harmonic resonance frequency is solely the effect of the liquid compressibility. If blood plasma is treated as an incompressible

liquid, $f_1$ is calculated from Eq. (32). According to this equation, $f_1$ tends to infinity when the bubble radius approaches the critical value ($R_{crit} = 2.24$ $\mu$m for Nycomed microbubbles). However, Nycomed microbubbles oscillating in blood plasma are not able to produce the resonance peak in the first-harmonic scattering cross-section if the transmitted frequency exceeds 14.33 MHz. The existence of the upper limit to $f_1$ results in another value of the critical bubble radius, specific for $f_1$. In particular, the resonant backscatter from Nycomed bubbles of radius less than $R_{crit1} = 2.54$ $\mu$m seems not to exist.

In the most experimental works on contrast agents, the properties of microbubbles, such as the shell viscosity and elasticity,[25,30] are evaluated through frequency analysis of the backscattered echo, i.e., from the output-level versus frequency curves. It is generally believed[1,31] that the highest peaks in these curves are associated with the resonance frequency of microbubbles. In reality, the highest peaks are associated with the first-harmonic resonance frequency of the backscattered signal $f_1$, which is not coincident with the microbubble resonance frequency $f_{res}$. Moreover, it is believed that the frequency at which the highest peak is observed depends on the microbubble parameters according to Eq. (18). In reality, equation (18) describes the undamped natural frequency $f_0$, which is different from the first-harmonic resonance frequency of the backscattered signal. The undamped natural frequency can be used instead of $f_1$ and $f_{res}$ if the microbubble radius is more than 5 $\mu$m, i.e., beyond the size range of contrast agents. Figure 5 shows how the difference between $f_1$ (measured in experiments) and $f_0$ (used instead of $f_1$) depends on the microbubble radius for two types of contrast agents: Nycomed[25,27] and Albunex®.[9] Although this difference is relatively small for bubbles of radius $R_0 = 5$ $\mu$m, in particular, $f_1 - f_0 = 0.34$ MHz for Nycomed bubbles and $0.025$ MHz for Albunex® bubbles, it becomes very large when the bubble radius approaches the critical value $R_{crit1}$. Note that in the case of Albunex® bubbles the critical radius for $f_1$ is again more than the critical radius for $f_{res}$: $R_{crit1} = 1.61$ $\mu$m $> R_{crit} = 1.46$ $\mu$m. The maximal difference between $f_1$ and $f_0$ is $8.8$ MHz for Nycomed bubbles and $14.1$ MHz for Albunex® bubbles. Therefore, the use of Eq. (18) for the interpretation of experimental data on the resonant backscatter from microbubbles cannot be tolerated.

A monodisperse suspension of encapsulated microbubbles cannot produce the resonant backscatter at both the transmitted frequency and twice the transmitted frequency. It is not quite correct to argue that if bubbles of one radius resonate, all the harmonics, subharmonics, and ultraharmonics of the backscattered signal they produce will be resonant. This statement is validated only for large bubbles. In particular, the second harmonic of the backscattered signal from encapsulated microbubbles of radius $R_0$ has a resonance peak at the frequency $f_2$ (second-harmonic resonance frequency), which is equal to neither the first-harmonic resonance frequency $f_1$ nor the undamped natural frequency $f_0$. This is apparent from the maximization of the second-harmonic scattering cross-section $\sigma_{s2}$. It should be noted that $f_2$ is defined as the *transmitted frequency* at which the second harmonic of the backscattered sig-

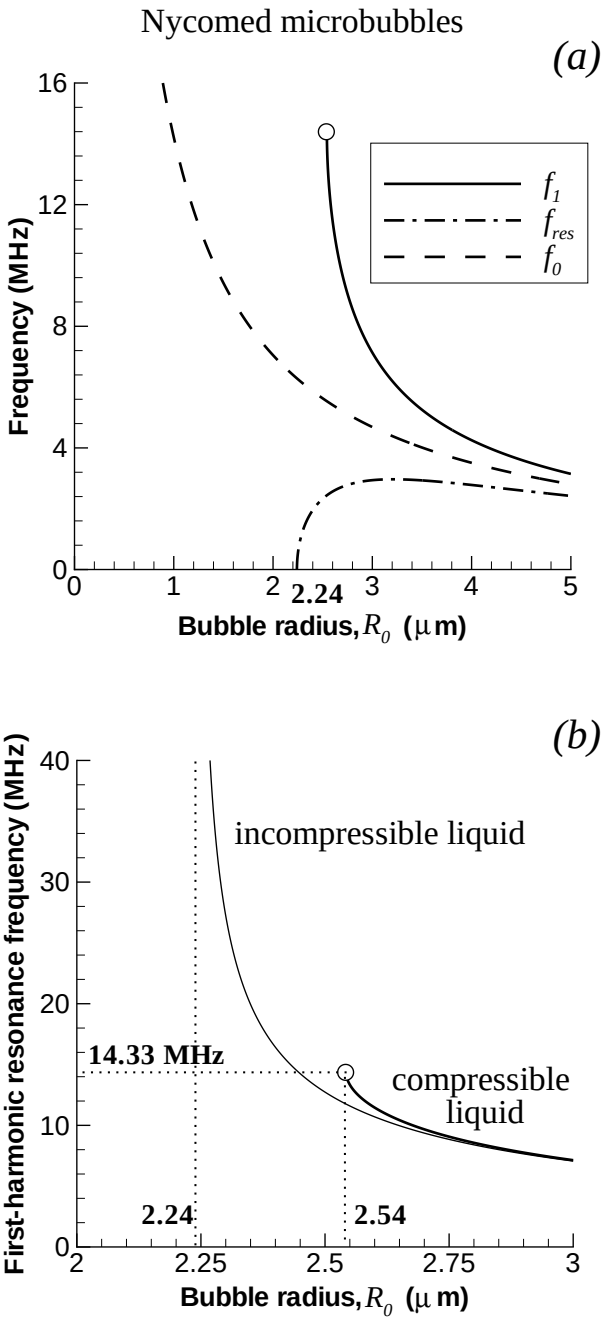


FIG. 4. (a) Resonance and undamped natural frequencies of Nycomed microbubbles (dash-dot and dashed) and first-harmonic resonance frequency of the backscattered signal from the microbubbles (solid line) as functions of the bubble outer radius. The liquid (blood plasma) compressibility is taken into account. Open circle denotes the highest frequency at which the resonant peak in the first-harmonic scattering cross-section can be observed. (b) The first-harmonic resonance frequency of the backscattered signal produced by Nycomed microbubbles surrounded by compressible and incompressible liquids (thick and thin solid lines) as a function of the bubble outer radius.

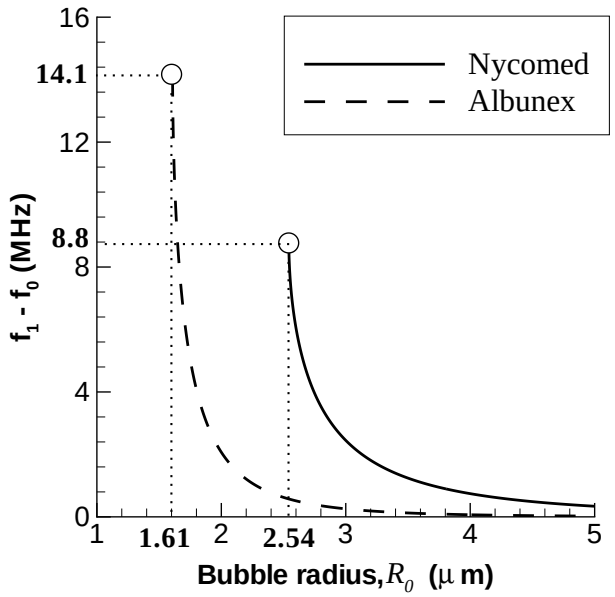


FIG. 5. The difference between the first-harmonic resonance frequency $f_1$ and the undamped natural frequency $f_0$ for Nycomed and Albunex® microbubbles (solid and dashed) as functions of the bubble outer radius. Nycomed microbubbles of radius $R_0 < 2.54$ $\mu$m and Albunex® microbubbles of radius $R_0 < 1.61$ $\mu$m do not produce resonant scattering at the transmitted frequency. The parameters are listed in Figs. 2 and 3.

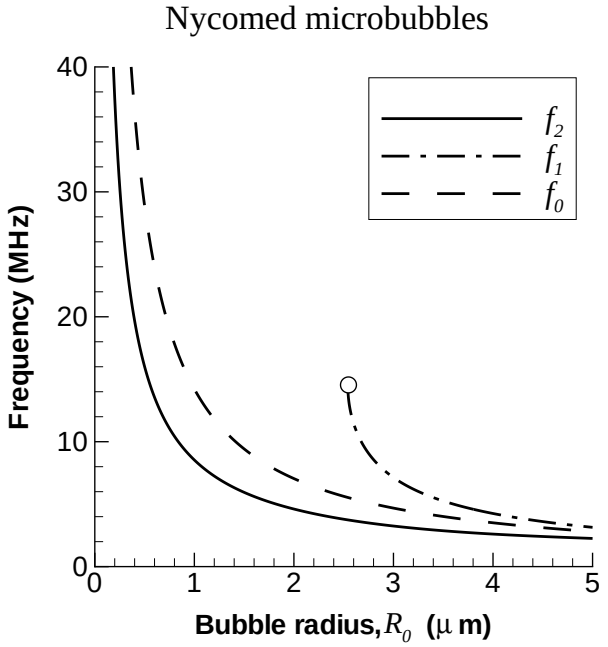


FIG. 6. First- and second-harmonic resonance frequencies of the backscattered signal (dash-dot and solid) and undamped natural frequency of Nycomed microbubbles (dashed) as functions of the outer radius. The liquid compressibility is taken into account. The second-harmonic resonance frequency is defined as the transmitted frequency at which the second harmonic of the backscattered signal is resonant. Open circle denotes the highest frequency at which the resonant peak in the first-harmonic scattering cross-section can be observed. $P_A = 30$ kPa. The remaining parameters are listed in Fig. 2.

nal is resonant, i.e., in the output-level versus frequency curve, the second-harmonic resonance peak will be at $2f_2$. The $\sigma_{s2}$ is a very complicated function of the angular frequency $\Omega$ [see Eq. (17b)]. It is impossible to obtain the analytical formula for $f_2$ even in the incompressible case. (If $T_{ac} = 0$, the maximization of $\sigma_{s2}$ results in a fifth-order algebraic equation in $\Omega^2$.) To calculate numerically the second-harmonic resonance frequency as a function of bubble radius, we use Maple™ (Maplesoft, a division of Waterloo Maple Inc.). The results of the numerical calculation are presented in Figs. 6 and 7.

Figure 6 compares the second-harmonic resonance frequency $f_2$ (solid line), the first-harmonic resonance frequency $f_1$ (dash-dot line), and the undamped natural frequency $f_0$ (dashed line) for Nycomed microbubbles of radius $R_0 \leq 5$ $\mu$m. While $f_1$ is always higher than $f_0$, $f_2$ is always less than $f_0$. Hence, the difference between $f_1$ and $f_2$ is more than between $f_1$ and $f_0$. It increases with decreasing the bubble radius. For instance, when the outer radius of Nycomed microbubbles is changed from $5$ $\mu$m to $2.54$ $\mu$m, $f_2 - f_1$ increases from $0.9$ MHz to $10.6$ MHz. Also, there is no critical radius for the second-harmonic resonance. Even submicron bubbles may have a resonance peak at twice the transmitted frequency. Hence, ultrasound-based methods for detection of very small bubbles inside materials should exploit the second harmonic, not the first harmonic.

As illustrated in Fig. 7, overestimation of the optimal transmitted frequency for second-harmonic imaging by using $f_0$ reaches several tens of MHz for microbubbles of radius less than $1$ $\mu$m. In this figure, the difference between $f_2$ and $f_0$ is plotted as a function of the outer radius for Nycomed and Albunex® microbubbles (solid and dashed lines). This difference remains relatively small (but cannot be ignored) for microbubbles of radius between $3$ $\mu$m and $5$ $\mu$m. In this range, $f_2 - f_0$ varies from $-0.55$ to $-1.43$ MHz for Nycomed bubbles and from $-0.063$ to $-0.485$ for Albunex® bubbles. The second-harmonic resonance frequency deviates significantly from the undamped natural frequency if the bubble radius is less than $3$ $\mu$m (or its size is less than $6$ $\mu$m).

The microbubble population is highly polydisperse. The polydisperse suspension is less sensitive to the transmitted frequency than the monodisperse suspension. If the ultrasound transducer operates at the frequency of several MHz (from $2$ to $14$ MHz), there always exist bubbles of one size, say $R_1$, that produce the resonant backscatter at the transmitted frequency and bubbles of another size, say $R_2$, that produce the resonant backscatter at twice the transmitted frequency. The backscattered signal from this suspension, therefore, has peaks at the transmitted frequency and multiple of this frequency. It is important to say that $R_1$ is not equal to $R_2$ in the case of encap-

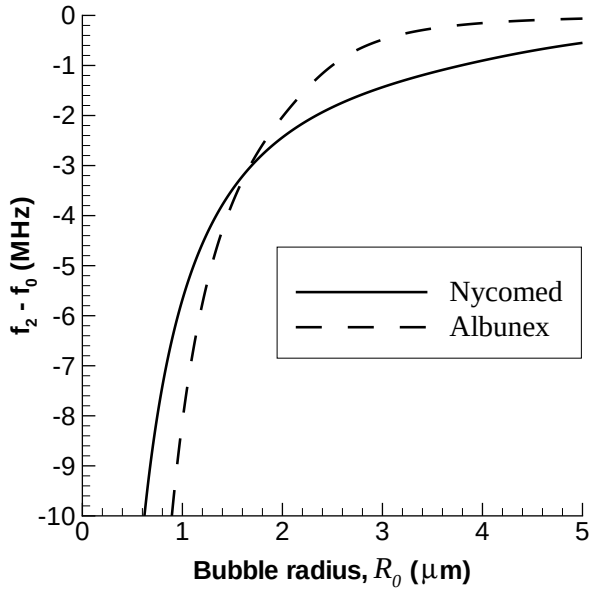


FIG. 7. The difference between the second-harmonic resonance frequency $f_2$ and the undamped natural frequency $f_0$ for Nycomed and Albunex® microbubbles (solid and dashed) as functions of the outer radius. $P_A = 30$ kPa. The remaining parameters are listed in Figs. 2 and 3.

sulated microbubbles.

To increase the quality of contrast-enhanced ultrasound imaging, one needs (a) to create a suspension of microbubbles with a mean radius equal to either $R_1$ (for fundamental mode imaging) or $R_2$ (for second-harmonic mode imaging) or (b) to operate the transducer at the frequency $f_1$ in the fundamental (first-harmonic) mode or at $f_2$ in the second-harmonic mode, where $f_1$ and $f_2$ are taken at the mean radius of microbubble population. The former way should be used if the transducer is characterized by a narrow range of operating frequencies. Unfortunately, neither Albunex® nor Nycomed (and other polymeric contrast agents) are good candidates for the fundamental mode imaging. The mean radius of Albunex® bubbles is about $1.7$ $\mu$m,[9] which is very close to the critical radius for $f_1$. As shown in Fig. 5, $R_{crit1} = 1.61$ $\mu$m for Albunex®. (The critical radius will be even higher if thermal damping is taken into account.) Polymeric microbubbles are worse than Albunex® because of the thick shell. The mean radius of Nycomed microbubbles is between $2.0$ and $2.5$ $\mu$m,[27] less than the critical radius ($R_{crit1} = 2.54$ $\mu$m for Nycomed). These contrast agents can, however, be used for second-harmonic imaging. Figure 8(a) shows that if the transducer operates at frequency $f = 5.0$ MHz (this frequency was used in experiments with Nycomed bubbles by Hoff *et al.*),[25] a Nycomed suspension should be of mean radius $R_1 = 4.36$ $\mu$m in order to provide optimal imaging in the fundamental (first-harmonic) mode. Such a high value of $R_1$ signifies that the major contribution to the first harmonic of the backscattered signal is from 4-5 $\mu$m bubbles, i.e., from the largest microbubbles of the suspension. Smaller microbubbles plays an insignificant role for first-harmonic imaging. Optimal second-harmonic imaging is possible if the mean radius of the Nycomed suspension is $R_2 = 2.77$ $\mu$m. This value is sufficiently close to the actual mean radius of the Nycomed suspension (between $2.0$ and $2.5$ $\mu$m), i.e., Nycomed microbubbles will scatter ultrasound more or less efficiently at twice the transmitted frequency. Nevertheless, one can increase the quality of second-harmonic imaging from Nycomed microbubbles by a slight decrease in the transmitted frequency. As illustrated in Fig. 8(b), the optimal transmitted frequency for second-harmonic imaging is $f_2 = 4.61$ MHz, if the mean radius of Nycomed microbubbles is $2.0$ $\mu$m. Figure 8(b) also shows that there is no optimal frequency for first-harmonic imaging. This is because $2.0$ $\mu$m is less than the critical radius $R_{crit1} = 2.54$ $\mu$m. It is necessary to say that the present analysis is expected to hold quantitatively for experiments on scattering by microbubbles under low-intensity continuous ultrasound. Finite-amplitude effects and polychromaticity of the ultrasound signal can lead to additional shifts in resonance frequencies.[13]

Because a lipid monolayer is very thin as compared to a polymeric or protein layer, the viscoelastic solid shell model does not work well for lipid-coated microbubbles. In this case, a Newtonian interface model suggested by Chatterjee and Sarkar[32] is more appropriate. This model introduces the interfacial dilatational viscosity $\kappa_s$ instead of the shell viscosity $\mu_s$. (In this model, an encapsulated shell has zero thickness.) Therefore lipid-coated microbubbles can be considered as free microbubbles with the decreased surface tension coefficient and the liquid viscosity replaced by

$$\mu_{lb} = \mu_l + \frac{\kappa_s}{a_0} \tag{35}$$

[see Eqs. (16) and (17) in Ref. 32]. Hence the viscous damping coefficient for lipid-coated microbubbles is calculated from Eq. (37), given below, where $\mu_{lb}$ is used instead of $\mu_l$. The viscosity-induced shift in resonance frequency will clearly exist for these microbubbles because the second term in the right-hand side of Eq. (35) becomes very large when bubble sizes are in micron or submicron range.

## III. FREE MICROBUBBLES

Another type of the commercially available ultrasound contrast agents represents emulsions that transform itself into suspensions of free gas microbubbles inside the human body.[1] In particular, Echogen (Sonus Pharmaceuticals, Bothell, Washington) is an emulsion of liquid dodecafluoropentane (DDFP) which boils at about $28^\circ$C.[1] In the liquid phase, such an emulsion is stable against dissolution. In the gas phase, it is more echogenic than a suspension of encapsulated microbubbles.

To evaluate backscattering by Echogen microbubbles at the transmitted frequency and twice the transmitted frequency, we can still use Eqs. (17) in which $R_0 = a_0$, $\sigma_1 = \sigma_2 = \sigma$, $Z = 0$, $p_{g0} = p_0 + 2\sigma/a_0$ (without the stabilizing layer, there is the over-pressure in the gas inside a microbubble), $\tau_{rr}^{(s)} = 0$,

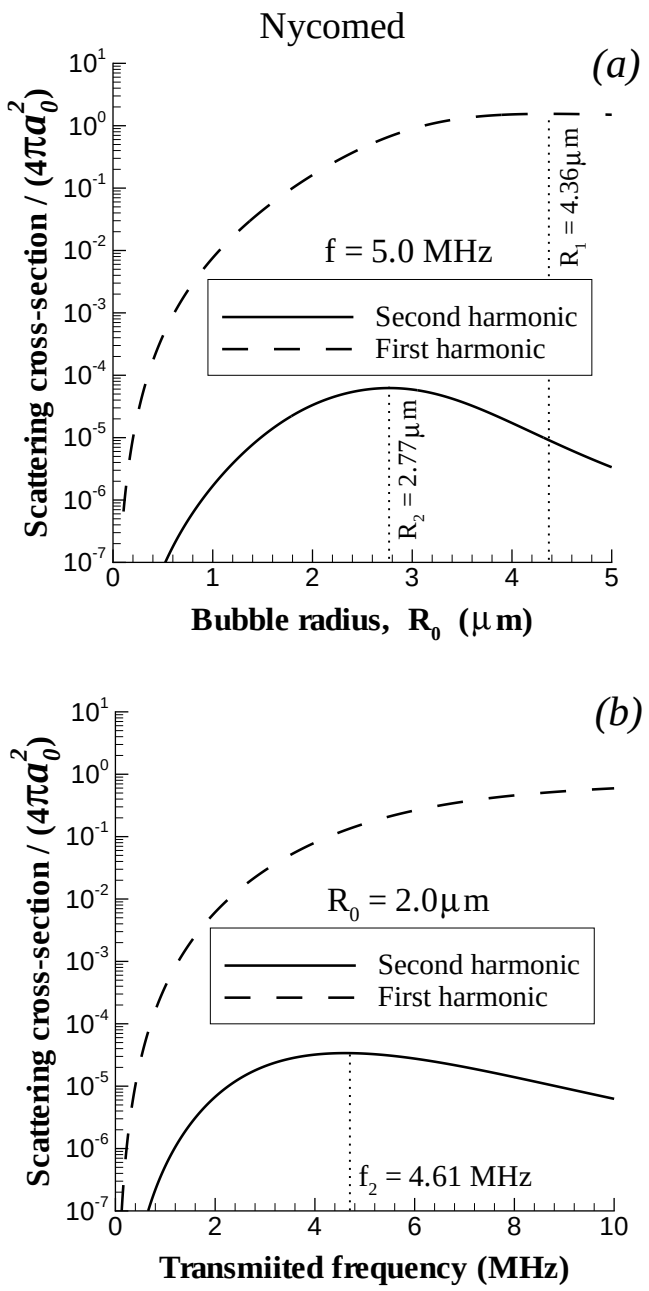


FIG. 8. First- and second-harmonic scattering cross-sections normalized by $4\pi a_0^2$ (dashed and solid) as functions of (a) bubble radius $R_0$ at the transmitted frequency $f = 5.0$ MHz and (b) transmitted frequency at $R_0 = 2.0$ $\mu$m. The parameters correspond to Nycomed microbubbles situated in blood plasma.

$\rho_{s0} = \rho_{l0}$, and $\Delta_\rho = 0$. In this case, the undamped natural frequency $f_0$ and the characteristic time $T_{ac}$ are given by

$$f_0 = \frac{1}{2\pi a_0}\sqrt{\frac{3\kappa p_0}{\rho_{l0}} + (3\kappa - 1)\frac{2\sigma}{\rho_{l0} a_0}}, \quad T_{ac} = \frac{a_0}{C_l}. \tag{36}$$

The viscous damping coefficient

$$\beta_{vis} = \frac{2\mu_l}{\rho_{l0} a_0^2}. \tag{37}$$

The expressions for $S_{ac}(\Omega)$ and $\beta_{ac}(\Omega)$ remain unchanged [see Eqs. (19) and (21)].

The viscous damping coefficient of free microbubbles is smaller than that of encapsulated microbubbles. For example, a free bubble of radius 1 $\mu$m situated in blood plasma ($\rho_{l0} = 1027$ kg·m$^{-3}$, $\mu_l = 0.0012$ Pa·s) is characterized by $\beta_{vis} \approx 2.337\times 10^6$ s$^{-1}$, while the viscous damping coefficient of an Albunex® microbubble of the same (outer) radius is approximately $1.596 \times 10^8$ s$^{-1}$. Therefore, the deviation of the resonance frequency from the undamped natural frequency is expected to be less for Echogen than for Albunex®. However, it is not negligible. Like encapsulated bubbles, free bubbles are characterized by a critical radius for bubble resonance $R_{crit}$. From (31) it follows that

$$R_{crit} = \left(\frac{3\kappa - 1}{3\kappa}\right)\frac{\sigma}{p_0}\left[-1 + \sqrt{1 + \frac{24\kappa\mu_l^2 p_0}{(3\kappa-1)^2\sigma^2\rho_{l0}}}\right] \tag{38}$$

for free bubbles. If $\sigma = 0$, the critical radius varies directly with the liquid viscosity $\mu_l$:

$$R_{crit} = \frac{2\sqrt{2}\,\mu_l}{\sqrt{3\kappa p_0 \rho_{l0}}}. \tag{39}$$

The liquid viscosity has a more effect on the critical radius than the surface tension. According to Eq. (38), if the surface tension increases from 0 to 0.04 N·m$^{-1}$, the critical radius of bubbles oscillating almost isothermally ($\kappa = 1.1$) in blood plasma decreases from 184 to 56 nm. An increase in the liquid viscosity from 0.0012 to 0.004 Pa·s (high-shear-rate viscosity of blood) at $\sigma = 0.04$ N·m$^{-1}$ leads to increasing $R_{crit}$ from 56 to 396 nm. Because the mean radius of Echogen microbubbles is about 75 nm,[17] a slight increase in viscosity and/or a decrease in surface tension, induced by soluble polymers and another surface-active molecules in blood, will make this suspension nonresonant. Experiments[17] show no first-harmonic resonance of the backscattered signal from these microbubbles. Note that the presence of a thin surfactant layer on the bubble surface, which is realized in lipid-shelled contrast agents and leads to a decrease in surface tension, will further magnify the critical radius and hence the difference between $f_0$ and $f_{res}$.

As illustrated in Fig. 9, the undamped natural frequency $f_0$ (dotted line) should not be used as the microbubble resonance frequency $f_{res}$ (solid line) for free bubbles in blood plasma if the bubble radius is less than 0.5 $\mu$m. Also, in this size range, both the first- and second-harmonic resonance frequencies of the backscattered signal $f_1$ and $f_2$ (dash-dot and dashed lines) deviate strongly from the undamped natural frequency. In particular, $f_1 - f_0$ and $f_0 - f_2$ are equal to 0.28 MHz and 0.61 MHz at $a_0 = 0.5$ $\mu$m but become 32.3 MHz and 24.8 MHz at $a_0 = 0.1$ $\mu$m. The critical radius for $f_1$ at which the first resonance frequency reaches the upper limit (357 MHz) is 66 nm.

## IV. CONCLUSION

The transmitted frequency at which the resonant excitation of microbubble oscillation occurs is taken to be equal to the

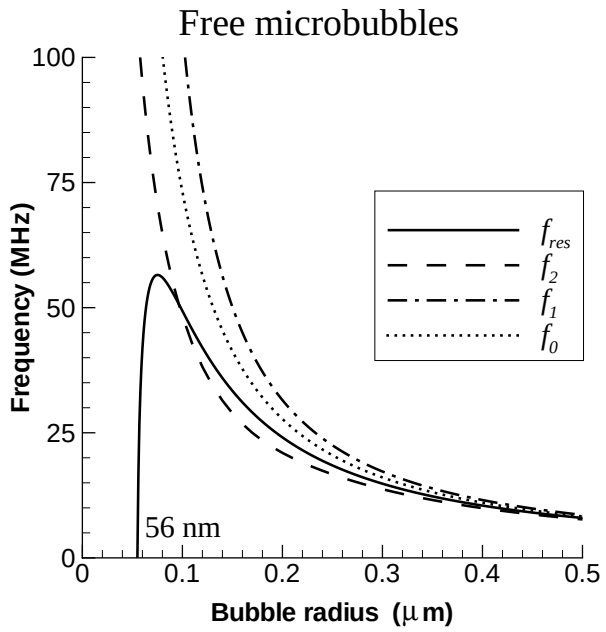


FIG. 9. Resonance and undamped natural frequencies of free microbubbles in blood plasma (solid and dotted) and first- and second-harmonic resonance frequencies of the backscattered signal from the microbubbles (dash-dot and dashed) as functions of the bubble radius. The blood plasma compressibility is taken into account ($C_l = 1543$ m·s$^{-1}$ and $\rho_{l0} = 1027$ kg·m$^{-3}$). The pressure wave amplitude $P_A = 30$ kPa. Other parameters: $\sigma = 0.04$ N·m$^{-1}$, $\mu_l = 0.0012$ Pa·s, $p_0 = 0.1$ MPa, and $\kappa = 1.1$. Free bubbles do not resonate if their size is less than $R_{crit} = 56$ nm. The upper limit to the first-harmonic resonance frequency $f_1$ is 357 MHz (not shown here). The critical radius for the resonant backscatter at the first harmonic is $R_{crit1} = 66$ nm.

undamped natural frequency in most experimental and theoretical works on scattering by contrast agents. We have shown that this assumption does not work for both free and encapsulated microbubbles used in contrast-enhanced ultrasound imaging. The resonance frequency of microbubbles deviates from the undamped natural frequency due to the increased viscous damping coefficient. The difference between these two frequencies rises as the bubble size decreases because the viscous damping coefficient is inversely proportional to the square of the bubble radius. The linear resonance of microbubble oscillation is characterized by a critical radius below which it cannot be observed. The critical radius of encapsulated microbubbles is typically between 1 and 3 $\mu$m and increases with increasing the shell thickness. The critical radius of free bubbles depends significantly on the liquid viscosity and surface tension. In blood plasma, free bubbles cease to resonate if their radius is below 56 nm.

The deviation of the resonance frequency from the undamped natural frequency results in the resonant backscatter by nonresonating microbubbles. The resonances of the backscattered signal (resonance peaks in the output-level versus frequency curves) are characterized by the frequencies different from both the microbubble resonance frequency and the undamped natural frequency. Every harmonic of the backscattered signal has its own resonance frequency. In particular, a monodisperse suspension of microbubbles cannot produce the resonant backscatter at both the trasmitted frequency and twice the transmitted frequency. (Because a microbubble suspension is polydisperse, there exist bubbles of one size that produce the resonant backscatter at the transmitted frequency and bubbles of another size that produce the resonant backscatter at twice the transmitted frequency.) The difference between the first- and second-harmonic resonance frequencies of the backscattered signal $f_1$ and $f_2$ reaches several MHz in the case of encapsulated microbubbles of radius less than 3 $\mu$m. To increase the quality of contrast-enhanced ultrasound imaging, the transducer should operate at the frequency $f_1$ in the fundamental mode and at the frequency $f_2$ in the second-harmonic mode, where $f_1$ and $f_2$ are taken at the mean radius of the ultrasound contrast agent.

Also, there exists a critical radius for the first-harmonic resonance of the backscattered signal, larger than the critical radius for the bubble resonance. The microbubbles of this radius produce the resonant backscatter at the transmitted frequency equal to the upper limit to the first-harmonic resonance frequency. There is no critical radius for the second harmonic resonance of the backscattered signal.

The resonance peak in the first harmonic of the backscattered signal is not observed in many experiments with ultrasound contrast agents. It is worth to mention Refs. 33 [Figs. 4, 5, and 7], 34 [Figs. 4(a) and 9(b)], and 25 [Fig. 5, see also Fig. 9]. The indirect evidence for the disappearance of the bubble resonance (and hence of the first-harmonic resonance of the backscattered signal) is presented in experiments by Chen *et al.*.[35] As noted by Hoff *et al.*,[25] "the resonance frequency increases and the resonance peak broadens and almost disappears due to the viscoelastic polymeric shell".

Our next concerns will incorporating bubble polydispersity and pulsed driving conditions (with different pulse shapes and lengths) into the theoretical model and performing a direct comparison between theoretical predictions and experimental data on the resonance frequencies of the backscattered signal from ultrasound contrast agents.

## ACKNOWLEDGMENTS

The author wishes to thank Ronald A. Roy and Ali Nadim for fruitful discussions. This work was partially supported by the North Atlantic Treaty Organization under Grant No. DGE-0000779. Any opinions, findings, conclusions or recommendations expressed in this publication are those of the author and do not necessarily reflect the view of NATO.

[1]D. Cosgrove, "Echo enhancers and ultrasound imaging," Eur. J. Radiol. **26**, 64–76 (1997).

[2]F. Calliada, R. Campani, O. Bottinelli, A. Bozzini, and M. G. Sommaruga, "Ultrasound contrast agents. Basic principles," Eur. J. Radiol. **27**, S157–S160 (1998).

[3]H. Becher and P. N. Burns, *Handbook of Contrast Echocardiography: Left Ventricular Function and Myocardial Perfusion* (Springer Verlag, New York, 2000).

[4]P. N. Burns, D. H. Simpson, and M. A. Averkiou, "Nonlinear imaging," Ultrasound Med. Biol. **26**, S19–S22 (2000).

[5]P. J. A. Frinking, A. Bouakaz, J. Kirkhorn, F. J. Ten Cate, and N. de Jong, "Ultrasound contrast imaging: Current and new potential methods," Ultrasound Med. Biol. **26**, 965–975 (2000).

[6]N. de Jong, P. J. A. Frinking, A. Bouakaz, M. Goorden, T. Schourmans, X. Jingping, and F. Mastik, "Optical imaging of contrast agent microbubbles in an ultrasound field with a 100-mhz camera," Ultrasound Med. Biol. **26**, 487–492 (2000).

[7]M. S. Plesset and A. Prosperetti, "Bubble dynamics and cavitation," Ann. Rev. Fluid Mech. **9**, 145–185 (1977).

[8]N. de Jong and L. Hoff, "Ultrasound scattering of Albunex® microspheres," Ultrasonics **31**, 175–181 (1993).

[9]C. C. Church, "The effects of an elastic solid surface layer on the radial pulsations of gas bubbles," J. Acoust. Soc. Am. **97**, 1510–1521 (1995).

[10]C. T. Chin and P. N. Burns, "Predicting the acoustic response of a microbubble population for contrast imaging in medical ultrasound," Ultrasound Med. Biol. **26**, 1293–1300 (2000).

[11]D. B. Khismatullin and A. Nadim, "Radial oscillations of encapsulated microbubbles in viscoelastic liquids," Phys. Fluids **14**, 3534–3557 (2002).

[12]J. S. Allen, D. E. Kruse, P. A. Dayton, and K. W. Ferrara, "Effect of coupled oscillations on microbubble behavior," J. Acoust. Soc. Am. **114**, 1678–1690 (2003).

[13]D. L. S. Hilgenfeldt and M. Zomack, "Response of bubbles to diagnostic ultrasound: a unifying theoretical approach," Eur. Phys. J. B **4**, 247–255 (1998).

[14]T. G. Leighton, *The Acoustic Bubble* (Academic Press, London, 1994).

[15]C. E. Brennen, *Cavitation and Bubble Dynamics* (Oxford University Press, New York, 1995).

[16]A. L. Klibanov, "Targeted delivery of gas-filled microspheres, contrast agents for ultrasound imaging," Advanced Drug Delivery Reviews **37**, 139–157 (1999).

[17]E. C. Everbach, R. A. Roy, and J. T. Flaherty, "Quantification of submicron DDFP gas bubbles using 30 mhz backscattered ultrasound," J. Acoust. Soc. Am. **110**, 2615 (2001).

[18]R. E. Apfel, "Radiation and ultrasound-triggered bubble contrast agents based on superheated drops," J. Acoust. Soc. Am. **108**, 2518 (2000).

[19]P. S. Epstein and M. S. Plesset, "On the stability of gas bubbles in liquid-gas solutions," J. Chem. Phys. **18**, 1505–1509 (1950).

[20]R. B. Bird, R. C. Armstrong, and O. Hassager, *Dynamics of Polymeric Liquids, Vol. 1: Fluid Mechanics* (Wiley, New York, 1987).

[21]I. S. Akhatov, N. K. Vakhitova, G. Y. Galeyeva, R. I. Nigmatulin, and D. B. Khismatullin, "Weak oscillations of a gas bubble in a spherical volume of compressible liquid," PMM J. Appl. Math. Mech. **61**, 921–930 (1997).

[22]R. I. Nigmatulin, I. S. Akhatov, N. K. Vakhitova, and J. R. T. Lahey, "On the forced oscillations of a small gas bubble in a spherical liquid-filled flask," J. Fluid Mech. **414**, 47–73 (2000).

[23]A. Prosperetti and A. Lezzi, "Bubble dynamics in a compressible liquid. Part 1. First-order theory," J. Fluid Mech. **168**, 457–478 (1986).

[24]W. T. Coakley and L. N. Nyborg, "Cavitation: Dynamics of gas bubbles: Application," in *Ultrasound: Its Applications in Medicine and Biology: Part 1*, edited by F. J. Frey (Elsevier, New York, 1978), pp. 77–159.

[25]L. Hoff, P. C. Sontum, and J. M. Hovem, "Oscillations of polymeric microbubbles: Effect of the encapsulating shell," J. Acoust. Soc. Am. **107**, 2272–2280 (2000).

[26]A. Prosperetti, "Thermal effects and damping mechanisms in the forced radial oscillations of gas bubbles in liquids," J. Acoust. Soc. Am. **61**, 17–27 (1977).

[27]K. Bjerknes, P. Sontum, G. Smistad, and I. Agerkvist, "Preparation of polymeric microbubbles: Formulation studies and product characterization," Int. J. Pharm. **158**, 129–136 (1997).

[28]T. D. Mast, "Empirical relationship between acoustic parameters in human soft tissues," ARLO **1**, 37–42 (2000).

[29]M. Abramowitz and I. A. Stegun, *Handbook of Mathematical Functions with Formulas, Graphs, and Mathematical Tables* (Dover, New York, 1972).

[30]N. de Jong, "Acoustic properties of ultrasound contrast agents," Ph.D. thesis, Erasmus Univresity, Rotterdam, The Netherlands, 1993.

[31]D. L. Miller, "Frequency relationships for ultrasonic activation of free microbubbles, encapsulated microbubbles, and gas-filled micropores," J. Acoust. Soc. Am. **104**, 2498–2505 (1998).

[32]D. Chatterjee and K. Sarkar, "A newtonian rheological model for the interface of microbubble contrast agents," Ultrasound Med. Biol. **29**, 1749–1757 (2003).

[33]P. J. A. Frinking and N. de Jong, "Acoustic modeling of shell-encapsulated gas bubbles," Ultrasound Med. Biol. **24**, 523–533 (1998).

[34]P. J. A. Frinking, N. de Jong, and E. I. Cespedes, "Scattering properties of encapsulated gas bubbles at high ultrasound pressures," J. Acoust. Soc. Am. **105**, 1989–1996 (1999).

[35]W.-S. Chen, T. J. Matula, and L. A. Crum, "The disappearance of ultrasound contrast agents: Observations of bubble dissolution and cavitation nucleation," Ultrasound Med. Biol. **28**, 793–803 (2002).